Probabilistic Simulation of Solidification Microstructure Evolution During Laser-Based Metal Deposition

Jingwei Zhang[1], Frank Liou[1], William Seufzer[3], Joseph Newkirk[2], Zhiqiang Fan[1], Heng Liu[1], Todd E.Sparks[1]

[1]Department of Mechanical and Aerospace Engineering,
Missouri University of Science and Technology
[2]Department of Metallurgical Engineering,
Missouri University of Science and Technology
[3]National Aeronautics and Space Administration

Accepted August 16th 2013

Abstract

A predictive model, based on a Cellular Automaton (CA) - Finite Element (FE) method, has been developed to simulate microstructure evolution during metal solidification for a laser based additive manufacturing process. The macroscopic FE calculation was designed to update the temperature field and simulate a high cooling rate. In the microscopic CA model, heterogeneous nucleation sites, preferential growth orientation and dendritic grain growth kinetics were simulated. The CA model was able to show the entrapment of neighboring cells and the relationship between undercooling and the grain growth rate. The model predicted the dendritic grain size, structure, and morphological evolution during the solidification phase of the deposition process. Model parameters for the simulations were based on stainless steel 316 (SS 316).

1. Introduction

As shown in Figure 1, laser deposition systems use a focused laser heat source to generate a molten pool on a substrate and melt injected powder thus creating a fully dense deposited bead. Solidification thermodynamics affect microstructure evolution, which directly affects materials mechanical properties. Several approaches have been taken to model microstructure evolution. A Monte Carlo stochastic method was shown by Anderson *et al*. [1], but this method does not explicitly consider the relationship between the growth rate of dendrite tips and undercooling. A phase field method was used by Choudhury *et al*. [2], but this method carried a high computational cost because of a requirement for a very fine computational grid. Another method employs a Cellular Automaton (CA) method proposed by Rappaz and Gandin [3]. The CA algorithm characterizes

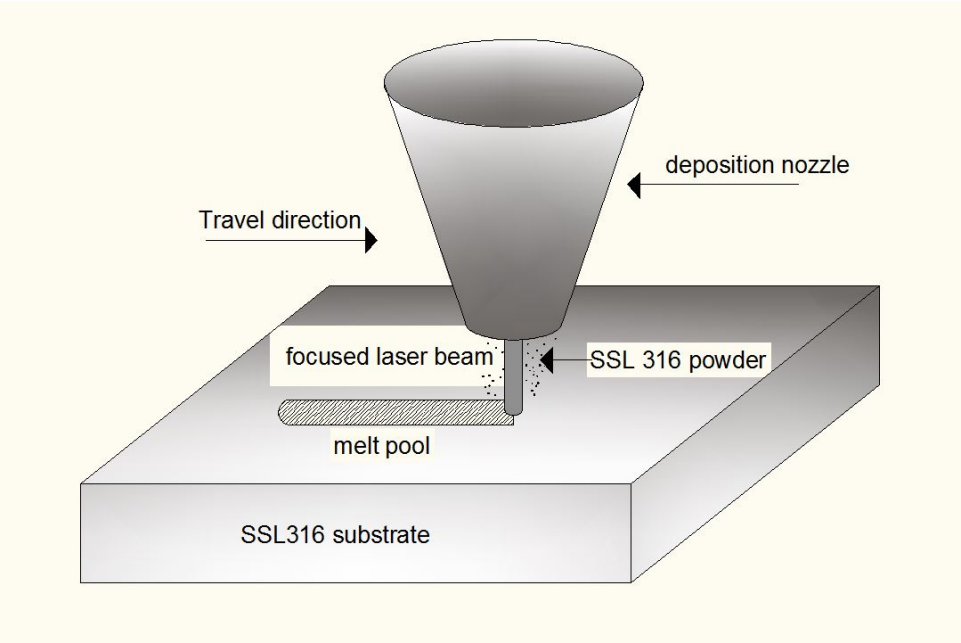

Figure 1: Schematic of LAMP laser deposition process

the discrete temporal and spacial microstructural evolution by utilizing a network of regular cells [4]. The advantages of the CA model are that it is based on a strict physical mechanism and has a low computation cost. The CA model can be coupled with a macroscopic thermal model to consider heat and mass transfer in complex geometries. The Cellular Automaton (CA) method for prediction of microstructure development was used to simulate the microstructure. In this model, CA was applied for predicting the dendritic grain size, shape and orientation evolution during the solidification phase of the deposition process.

2. Mathematical Model

The mathematical approach taken in this study involves two models. Nucleation and grain growth are implemented at a microscopic level with a CA method. Since nucleation and grain growth are driven by temperature, a macroscopic thermal model, based on a Finite Element (FE) method, is used. Macroscopic and microscopic are used to highlight that these models run at two different scales in time and space. The CA and FE models, and how they are coupled, are described in the following sections.

2.1 Microscopic CA Model

2.1.1 Nucleation

Heterogeneous nucleation occurs nearly instantaneously at a characteristic undercooling. The locations and crystallographic orientation of the new nuclei are randomly chosen at the surface or in the liquid. As explained by Oldfield [5], the continuous nucleation distribution, $\mathrm{d}n/\mathrm{d}\Delta\mathrm{T}^{'}$, which characterizes the relationship between undercooling and the grain density, is described by a Gaussian distribution both at the mould wall and in the bulk liquid (Eq.(1)). The parameters of these two distributions, including maximum nucleation density $n_{\max}$, the mean undercooling ΔT_N, and the standard deviation of the grain density distribution ΔT_σ, can be obtained from experiments and grain size measurements. The grain density, $n(\Delta T)$, is given by (Eq.(1)):

$$n(\Delta T) = \int_0^{\Delta T} \frac{\mathrm{d}n}{\mathrm{d}\Delta T^{'}} \mathrm{d}\Delta T^{'} = \int_0^{\Delta T} \frac{n_{max}}{\Delta T_\sigma \sqrt{2\pi}} \exp\left[-\frac{1}{2}\left(\frac{\Delta T^{'} - \Delta T_N}{\Delta T_\sigma}\right)\right] \mathrm{d}\Delta T^{'} \tag{1}$$

where $n_{\max}$ is the maximum nucleation density of nucleation grains, which is obtained by the integral of the nucleation distribution (from zero undercooling to infinite undercooling). ΔT_N and ΔT_σ are the mean undercooling and standard deviation of the grain density distribution, respectively. Here, all temperatures are in Kelvin.

According to the cellular automaton algorithm used by M.Rappaz *et al*. [3](Eq.(2)), if the nucleation probability $p_v = \delta n_v V_{CA}$ equals or exceeds a random number r $(0 \leqslant r \leqslant 1)$ during the time step δt, the cell will nucleate instantaneously.

$$p_v \geqslant r \tag{2}$$

Here, δn_v is the grain density increase, and V_{CA} is one CA cell volume.

2.1.2 Grain Growth

In the case of alloy dendritic growth from the undercooled melt, the coupled transport (solute and heat) problem must be solved. The model considers the marginal stability and capillarity effect. The total undercooling of the dendritic tip consists of three parts, solute undercooling, thermal undercooling and curvature undercooling. For most metallic alloys, the kinetic undercooling for atom attachment is small so it is neglected [6]. The total undercooling can be calculated by (Eq.(3)).

$$\Delta T = mC_0[1 - A(P_c)] + \theta_t I(P_t) + \frac{2\Gamma}{R} \tag{3}$$

where m is the liquidus slope; Γ is the Gibbs-Thomson coefficient; C_0 is the solute concentration in the liquid far from the solid-liquid interface; P_t and P_c are the thermal and solutal Péclet numbers, respectively; k is the solute partition coefficient at the solid-liquid interface; $A(P_c)$ equals $[1-(1-k)I(P_c)]^{-1}$; θ_t is the unit thermal undercooling ($=\Delta h_f/c$); and R is the radius of the dendritic tip.

In equation (3), k , D and Γ depend on the temperature. Here, the following model built by Aziz *et al*. [7] was used:

$$k = \frac{k_0 + (a_0 V/D_i)}{1 + (a_0 V/D_i)} \tag{4}$$

where k_0 is the equilibrium partition ration, D_i is the interface diffusion coefficient in the liquid, and a_0 is a length scale associated with the interatomic distance and is estimated to be between 0.5 and 5 nm.

A dendritic tip with a parabolic shape was applied in this model, expressed in its simple form as:

$$\Omega = \mathrm{I}(P) \tag{5}$$

where Ω represents supersaturation, and the Ivantsov function(the function of Peclet number P) for a needle crystal associated with the parabolic dendritic tip is provided by:

$$\mathrm{I}(P) = P\exp(P)\mathrm{E}_1(P) \tag{6}$$

where $\mathrm{E}_1(P)$ corresponds to the exponential integral function.

$$\mathrm{E}_1(P) = \int_P^{+\infty} \frac{\exp(-z)}{z}\mathrm{d}z \tag{7}$$

Langer and M*ü*ller-Krumbhaar [8] proved that dendrite tips grow in marginally stable state. Therefore, we can write the approximate equation:

$$R = \lambda_i \tag{8}$$

where λ_i is the critical wavelength of the solid-liquid interface at the limit of stability. For the laser deposition process, the rapid solidification condition corresponds to a high Peclet number, at which, the dendritic tip radius is given by (Eq.(9)):

$$\mathrm{R} = \left[\frac{\Gamma}{\sigma^*(mG_c^* - G^*)}\right]^{1/2} \tag{9}$$

where σ^*, the marginal stability constant, approximately equals $1/(4\pi^2)$[9]. G^* and G_c^* are the effective temperature gradient and concentration gradient, respectively. By substituting G_c^* and G^*, the dendritic tip radius, R, is calculated by

$$\mathrm{R} = \frac{\Gamma/\sigma^*}{\theta_t P_t \xi_t + 2\theta_c P_c \xi_c} \tag{10}$$

where $\theta_c = \Delta T_0 kA(P_c)$, and ξ_t and ξ_c are defined as in [6]. The growth velocity and the dendrite tip radius were calculated using an iterative method [10].

For columnar dendrite growth, the effect of latent heat release can be neglected, so the imposed temperature field will not produce thermal undercooling. The full transport equation reduces to:

$$\Delta T = \Delta T_c + \Delta T_r \tag{11}$$

By substituting ΔT_c and ΔT_r in (Eq.(3)) and (Eq.(9)) into (Eq.(11)), one obtains the result:

$$\frac{\pi^2 \Gamma V^2}{P_c^2 D^2} + \frac{\theta_c \xi_c V}{D} + G = 0 \tag{12}$$

Equations (10) and (12) yield the relationship between R and V.

2.1.3 Cellular automaton simulation procedure

A time and space discreted cellular automaton (CA) method was used to develop the grain formation, as detailed in [3] and [11]. A network of equal size square cells was designed into the model. Each cell has different variables (temperature, crystallographic orientation and phase state). Each phase state index was given certain value. A state index of zero represented liquid, and a positive integer state index(from 1 to 48) represented solid and crystallographic orientations in 2D model.

During the grain growth, the 2D "decentred square" growth algorithm [12] was used to avoid overgrowth of the square envelope and maintain the original crystallographic orientation. The virtual growth center does not correspond to the cell center in the CA network. After a few time-steps of growth, the square envelope was truncated to an appropriate size, which will guarantee that the grain will not grow forever. This maintains the original orientation and guarantees the development of solidification microstructure under a non-uniform temperature field. The growth rate of the dendritic tips along four diagonal directions were independent because of the non-uniform temperature, resulting in final envelopes that were not strictly square. The capillarity effect, marginal stability, local undercooling and solute concentration are considered in the grain growth kinetics model.

The macroscopic model can provide temperature field information at each node. Here linear interpolation was used to obtain the finer temperature nodes because the finite element mesh for heat flow calculation was coarser than in the CA grids.

2.2 Macroscopic FE Thermal Model

In order to obtain the microstructure information during the solidification process, the temperature field must be known at each time step. The Finite Element Method (FEM) [13], which is appropriate for complex shapes with limited nodes, was selected here. A linearized implicit FE enthalpy formulation of the heat flow equation can be given by

$$\left[\frac{1}{\Delta t}\cdot[M]+[K]^t\cdot\left[\frac{\partial T}{\partial H}\right]^t\right]\cdot\{\delta H\}=-\{K\}^t\cdot\{T\}^t+\{b\}^t \tag{13}$$

where $\{M\}$ is the mass matrix; $\{K\}$ is the conductivity matrix; $\{b\}$ is the boundary condition vector; and $\{T\}$ and $\{H\}$ are the temperature and enthalpy vectors at each node of the FE mesh, respectively. The assumption here is that the conductivity matrix and boundary condition term do not vary much with time. The Newton Method and Euler implicit iteration are included in equation(13). This set of equations can be solved using the Gauss elimination method for $\{\delta H\}$.

$$\delta H=\rho\cdot c_p\cdot[T^{t+\delta t}-T^t]-\Delta H_f\cdot\delta f_s \tag{14}$$

Thus, the next time-step enthalpy can be obtained by the relationship $H_i^{t+1}=H_i^t+\delta H$. The new temperature field can be obtained from the coupling model using equation(14). δf_s can be calculated as in [14].

2.3 Coupling Macroscopic with Microscopic Model

In the FE macroscopic model, the temperature field was calculated on a relatively coarse mesh, but the solidification microstructure had to be developed on a finer regular CA mesh with a cell size of the order of the secondary spacing. The known temperature T_n^t and the volumetric enthalpy variation δH_n were interpolated into the CA network by the linear interpolation in Eqs (15). ϕ_{vn} is the interpolation coefficient.

$$T_v^t=\sum_n\phi_{vn}\cdot T_n^t,\ H_v^t=\sum_n\phi_{vn}\cdot H_n^t \tag{15}$$

The finer temperature, T_v^t, and enthalpy variations δH_v^t in regular CA cells were used in equation (14) to yield the temperature in the next micro time step. After a few micro time steps, the temperature field in the CA network could be substituted into the coarser nodes of the macroscopic model. In this case, the laser deposition process is considered a rapid solidification process, so the cooling rates were as high as $10^3\sim10^4K/s$ [15]. The macro time step for the FE model was of the order of $10^{-4}s$. An adaptive micro time step was $2\times10^{-5}s$ so that in each time step, the

temperature decrease is less than 0.2K. Thus the temperature and enthalpy fields were interpolated into the microstructure model in both space and time. The latent heat release in the microscopic model was interpolated back into the macroscopic model.

3. Results and Discussion

This section includes a discussion of the preliminary results of the macroscopic model (FEM) for the temperature. The solidification microstructure evolution of the coupling CA model under laser deposition of SS 316 is also discussed.

Figure 2 shows the temperature field evolution in the macroscopic model from the starting time, t=100ms, to the finishing time, t=150ms. It can be seen that the heat source moved towards right during this period. In Figure 2, the black rectangle represents the microscopic domain, which is the area portrayed in Figure 3 from the microscopic CA model.

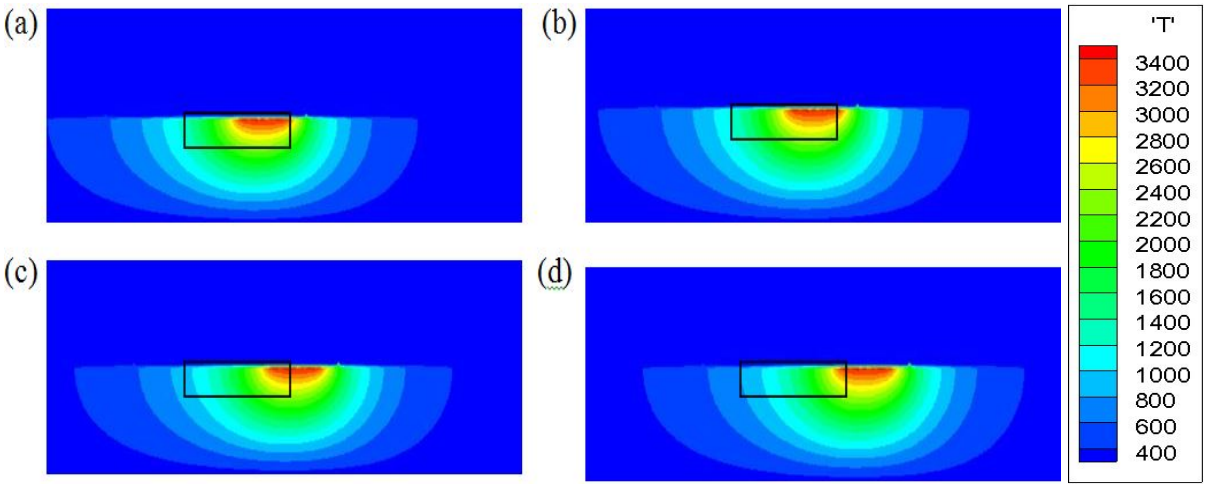

Figure 2: Macroscopic FE simulated temperature field for laser deposition of SS 316. Temperatures are in K and shown at a) t=105ms, b) t=120ms, c) t=135ms, and d) t=150ms. The black rectangle indicates section of thermal results used for the CA microscopic model. The rectangle is 200 μm wide and 70 μm high.

As Figure 2 illustrates, at the starting time, the hottest area was almost within the microscopic domain (i.e. the bold black rectangle in Figure 2(a)), and the temperature of most of the microscopic domain exceeded the liquidus temperature. Therefore; the majority of the melt pool had not solidified. After a 50ms evolution, the hottest area almost fell outside of the microscopic domain, and some parts of that domain had solidified because the temperature was below the liquidus temperature and hit the critical undercooling value.

Figure 3 shows the evolution of the solidification microstructure during the laser deposition process of SS 316. The grid size for the macroscopic model was 10μm, and the macro time step was $10^{-4}s$. The grid size for the microscopic model was 2μm, and the micro time step was $2 \times 10^{-5}s$.

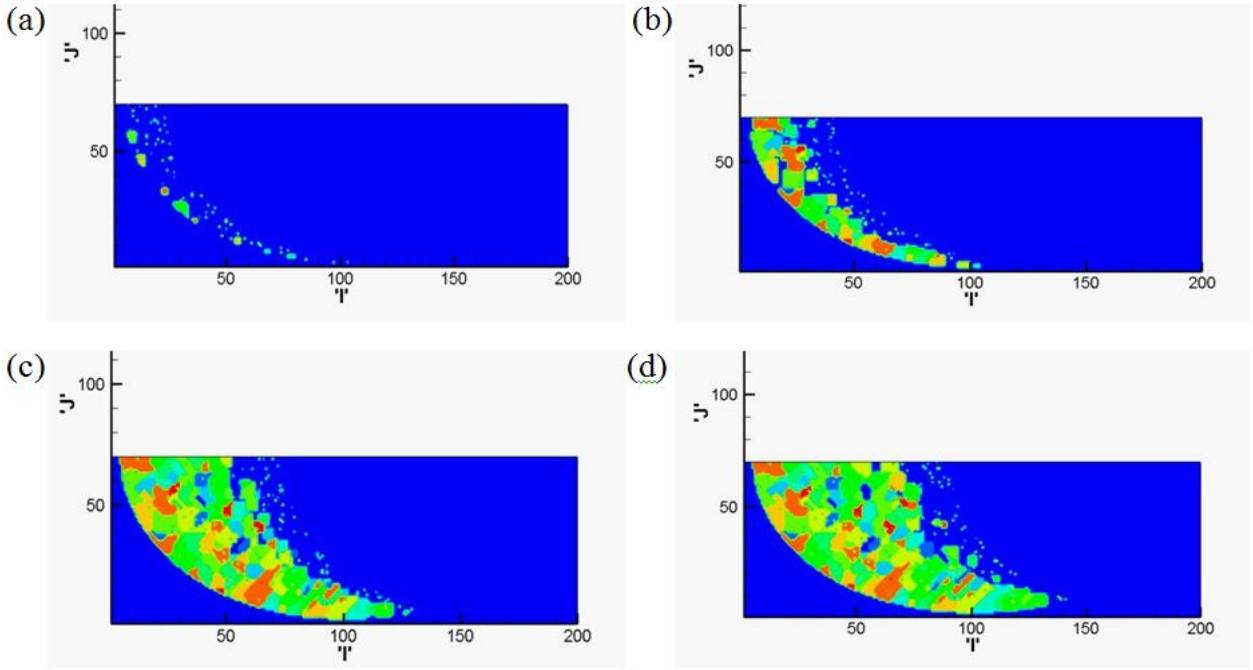

Figure 3: Microscopic CA simulation evolution of SS 316 microstructure during solidification. Microstructure evolution is shown at a) t=105ms, b) t=120ms, c) t=135ms, and d) t=150ms. 'I' and 'J' axes are in μm, depicting the grains length in two dimension. Color indicates individual grains.

As the Figure 3 illustrates, the grains initially nucleated at the interface between the solid and liquid because the heat transfer at the interface occured much faster than in the liquid. The different colors represent different crystallographic orientations of grains. Also, during grain growth, the grains always maintained their original orientations, which agreed with the physical mechanism.

These simulation results have not been compared with the results of laser deposition experiments. The grain size and shape need to be measured in such experiments in order to improve the simulation results. Additional DTA [16] experiments also must be conducted to find the critical parameters for describing the Gaussian distribution in detail. In the future, the current "2D decentred square algorithm" will be replaced by "3D decentred octahedron algorithm" [17] without affecting the cell grid superimposing to a coarser finite element mesh.

4. Conclusion

From the simulation results, the coupled model described in this paper can approximate the temperature field of the substrate, the melt pool, solidification, and the microstructure evolution of SS 316 during the laser deposition process. The FE model provides the temperature at a relatively coarse scale and interpolation is used to scale the temperature field to match that of the CA model. The CA model predicts microstructure evolution as the substrate cools. Hence, the instantaneous nucleation law, dendritic grain growth, and crystallographic orientation were modeled in this study. Future work will be directed into the development of a 3D FE and CA model.

Acknowledgements

This work was funded through NASA's Fundamental Aeronautics Program, Fixed Wing Project, under NRA NNX11AI73A. The authors would like to acknowledge Karen Taminger (NASA Langley Research Center) for her critical advice and mentorship.

References

[1] M. Anderson, D. Srolovitz, G. Grest, and P. Sahni, "Computer simulation of grain growthi. kinetics," *Acta metallurgica*, vol. 32, pp. 783–791, 1984.

[2] A. Choudhury, K. Reuther, E. Wesner, and A. August, "Comparison of phase-field and cellular automaton models for dendritic solidification in alcu alloy," *Computational Materials Science*, vol. 55, pp. 263–268, 2012.

[3] M.Rappaz and Ch.-A.Gandin, "Probabilistic modelling of microstructure formation in solidification processes," *Acta metal.mater.*, vol. 41, no. 2, p. 345, 1993.

[4] D. Raabe, "Cellular automata in materials science with particular reference to recrystallization simulation," *Annual Review of Materials Reviews*, vol. 32, pp. 53–76, 2002.

[5] W. Oldfield, "A quantitative approach to casting solidification: Freezing of cast iron," *Trans. Am. Soc. Metals*, vol. 59, p. 945, 1966.

[6] W.KURZ and D.J.FISHER, *Fundamentals of Solidification*, ch. Appendix 7 and 8, pp. 226–246. TRANS TECH PUBLICATION, 1992.

[7] K.A.Jackson, G.H.Gilmer, and H.J.Leamy, *Laser and Electron Beam Processing and Materials*, p. 104. New York: Academic Press, 1980.

[8] J.S.Langer and H. Krumbhaar, "Stability effect in dendritic crystal growth," *J.Cryst.Growth*, vol. 42, pp. 11–14, 1977.

[9] W.KURZ and D.J.FISHER, *Fundamentals of Solidification*, ch. Appendix 9, pp. 247–260. TRANS TECH PUBLICATION, 1992.

[10] Ch.-A.Gandin, G.Guillemot, B.Appolaire, and N.T.Niane, "Boundary layer correlation for dendrite tip growth with fluid flow," *Mater.Sci.Eng.A*, vol. A342, pp. 44–50, 2003.

[11] Ch.-A.GANDIN, R.J.SCHAEFER, and M.RAPPAZ, "Analytical and numerical predictions of dendritic grain envelopes," *Acta mater.*, vol. 44, no. 8, pp. 3339–3347, 1996.

[12] H. Zhang, K. NAKAJIMA, and R. WU, "Prediction of solidification microstructure and columnar-to-equiaxed transition of al-si alloy by two-dimensional cellular automaton with "decentred square" growth algorithm," *ISIJ International*, vol. 49, no. 7, pp. 1000–1009, 2009.

[13] Ph.THÉVOZ, J.L.DESBIOLLES, and M.RAPPAZ, "Modeling of equiaxed microstructure formation in casting," *METALLURGICAL TRANSACTIONS A*, vol. 20A, p. 311, February 1989.

[14] Ch.-A.GANDIN and M.RAPPAZ, "A coupled finite element-cellular automaton model for the prediction of dendritic grain structures in solidification," *Acta metall.mater*, vol. 42, no. 7, pp. 2233–2246, 1994.

[15] B.ZHENG, Y.ZHOU, and J.E.SMUGERESKY, "Thermal behavior and microstructure evolution during laser deposition with laser-engineered net shaping: Part ii. experimental investigation and discussion," *METALLURGICAL AND MATERIALS TRANSACTIONS A*, vol. 39A, p. 2237, 2008.

[16] J.A.Dantzig and M.Rappaz, *Solidification*, ch. 7, pp. 259–261. EPFL Press, first ed., 2009.

[17] C.-A. GANDIN, J.-L. DESBIOLLES, M. RAPPAZ, and P. THÉVOZ, "A three-dimensional cellular automatonfinite element model for the prediction of solidification grain structures," *METALLURGICAL AND MATERIALS TRANSACTIONS A*, vol. 30A, p. 3153, December 1999.